The Gulf of Cádiz Contourite Laboratory: Sediment variability from Recent to 300kya

Senior Thesis

Submitted in partial fulfillment of the requirements for the

Bachelor of Science Degree

At The Ohio State University

By

Sean O'Brien

The Ohio State University

2014

Approved by

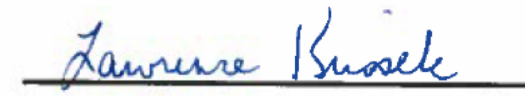

Lawrence A. Krissek, Advisor
School of Earth Sciences

ABSTRACT

Integrated Ocean Drilling Program Expedition 339 drilled contourite deposits in the Gulf of Cádiz and West Iberian margin. These recovered sedimentary successions provide key data for examining the development of the Mediterranean Outflow Water and the subsequent evolution of a complex contourite depositional system. In this study, the major terrigenous mineral phases at Sites U1387 and U1389 were identified to define sediment composition and interpret its provenance. Temporal changes in sediment composition are analyzed to ~300 kya to identify changes in provenance, continental weathering regimes, and/or dispersal patterns.

The shipboard age model was used to assign sediment ages using a constant sedimentation rate of 25 cm/ky for Site U1387 and 40 cm/ky for Site U1389. The samples investigated range from Recent to 300 kya, with a sampling interval of ~4 ky. Randomly mounted pressed powder samples were examined using x-ray diffractometry to identify bulk mineralogy. Semiquantitative mineral abundances in each sample are estimated by comparing the ratio of a mineral's selected peak area to that of the 4.26Å quartz peak.

Preliminary results show that the primary mineral phases include: quartz, calcite, dolomite, aragonite, feldspar, and a variety of clay minerals. This composition is consistent with onshore lithologies, as well as shipboard XRD results. At Site U1389, calcite and 7Å intensity ratios are higher in interglacial periods while dolomite decreases. Site U1387 samples show higher dolomite/quartz values in the glacial period measured (MIS 8). This illustrates preferential deposition of calcite and the 7Å clays during times of weakened MOW flow at a site, and preferential deposition of dolomite and quartz during times of strong MOW flow at a site. This difference in behavior may be controlled by the relatively smaller grain size of calcite and the 7Å clays compared to quartz and dolomite.

TABLE OF CONTENTS

ACKNOWLEDGEMENTS

I would like to express my thanks and gratitude to my research advisor, Dr. Lawrence Krissek. His expertise, guidance, and dedication strengthened my enthusiasm to conduct research and develop my skills in geology. I am also deeply appreciative of Erin Lathrop, who provided me with continuous support and consultation as we completed our projects. A special thanks goes out to Dr. Anne Carey for her coordination of the Shell Undergraduate Research Experience and for her welcome advice throughout the process of writing this thesis.

I also must acknowledge the contributions of Dr. Julie Sheets. My work in operating and troubleshooting the XRD, as well as interpreting profiles, would not have been possible without her assistance. Her suggestions of methods to interpret relative mineral abundances were also integral to the success of this project.

I recognize that this research would not have been possible without funding from Shell Exploration and Production Company under the Shell Undergraduate Research Experience internship program. Furthermore, I extend gratitude to the USSSP for providing funding for the XRD scans and to the Integrated Ocean Drilling Program for providing the samples for this project. The Friends of Orton Hall Fund and the Garry McKenzie Undergraduate Scholarship Fund are acknowledged for providing travel funds.

Most importantly, I must thank my family for their support and faith in my abilities throughout my undergraduate career. I am indebted to them for the confidence, integrity, and strength of will they have instilled in me in the course of my academic journey.

Finally, I thank Dr. Peter Pober and the rest of my family in Fairfax, Virginia for having taught me all I know about communication, friendship, and the power of words.

INTRODUCTION

The goal of this project was to investigate how mineralogy can be used as a proxy to interpret shifts in the paleocirculation of a bottom-water current in the Gulf of Cádiz. Known as the Mediterranean Outflow Water (MOW), the bottom-water current exits as a water mass at the Straits of Gibraltar, a narrow and shallow connection between the Atlantic Ocean and the Mediterranean Sea. The MOW influences the formation of the North Atlantic Deep Water, which impacts the Atlantic Meridional Overturning Circulation and subsequently, global thermohaline circulation. Yet despite the MOW's integral role in global climate variation, its influence is still poorly understood (Bozec et al., 2011).

From November 2011 to January 2012, Expedition 339 of the Integrated Ocean Drilling Program (IODP) drilled five sites in the Gulf of Cadiz. The expedition's objective was to determine what role the MOW's variability plays in global climate. In these areas of high sedimentation rates, bottom-water currents that flow along bathymetric contours have the ability to form expansive, laterally continuous sedimentary bodies called contourites. These deposits have recently become the subject of increasingly more research.

Despite their widespread distribution, contourite depositional systems in the Gulf of Cadiz and around the world have not received significant attention until recent years. Found on most continental margins, contourite deposits are widespread and abundant. However, proper identification can be a complex task, especially in ancient rock deposits now exposed on land. (Rebesco, 2014; Hunecke and Stow, 2008). Indeed, while a contourite facies model has existed since the early 1980s, modifications continue to be made as new information regarding these poorly understood deposits is uncovered (Stow and Faugères, 2008). The primary consistent factors among contourite facies models are two-fold: (1) pervasive bioturbation and (2)

bigradational grading: a coarsening upward sequence tied to an increase in current velocity, followed by a fining-upward sequence as a result of the successive decrease in current velocity (Figure 1).

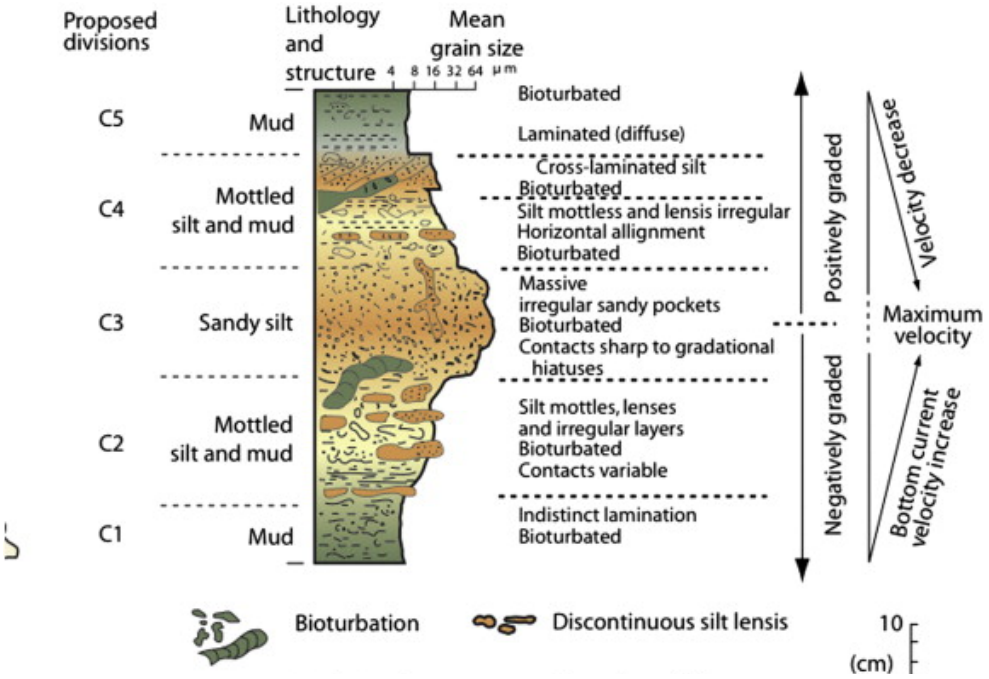

Figure 1 - Contourite facies model with shifts according to current velocity, from Stow and Faugères (2008)

An understanding of contourite deposits is significant for numerous areas of scientific interest. First, research on these deposits can assist with geohazard mitigation. The composition, structure, and locations of contourite deposits are all conducive to eventual liquefaction. This leads to slope instability and rapid subsea mass wasting events, exacerbated by the wide areal extent of these features (Lee and Baraza, 1999). These events can be catastrophic, especially in areas with subsea infrastructure. A better understanding of the processes that form these deposits will enhance our ability to identify the deposits most susceptible to failure.

Next, contourites are of great interest to paleoceanographers and paleoclimatologists. Located in areas with high sedimentation rates, these deposits provide continuous, high-

resolution records of various processes through time. They are an especially strong recorder of current activity, making them ideal for reconstructions of the MOW's variability.

Finally, some recent effort is motivated by the economic potential of contourite depositional complexes. The oil and gas industry is progressively exploring deeper waters. Thus, their research teams are significantly more attentive to depositional systems in those regions. This is for good reason, considering that current facies models and samples confirm that contourites have characteristics favorable to the formation of reservoirs, seals, and traps (Viana and Rebesco, 2007). Still, work in this field has been stalled largely due to the absence of indisputable criteria for identifying modern and ancient contourites. IODP Exp. 339 recovered thick, well-sorted contourite sands that are suited for reservoir potential, offering a promising future for this area of research (Expedition 339 Scientists, 2012).

STUDY GOALS

The large-scale variability of the Mediterranean Outflow Water has been relatively well defined, in contrast to the less frequently studied shorter scale variation of dominance between its upper and lower core positions (Penaud et al., 2010). This project's objective was to employ mineralogy to interpret shifts in MOW position in the Gulf of Cádiz from recent to ~300 kya. Initial goals were defined as:

1) Identify major terrigenous mineral phases at Site U1387 and Site U1389
2) Interpret mineralogy to reveal sediment provenance
3) Examine temporal variation in mineral abundance

GEOLOGIC SETTING

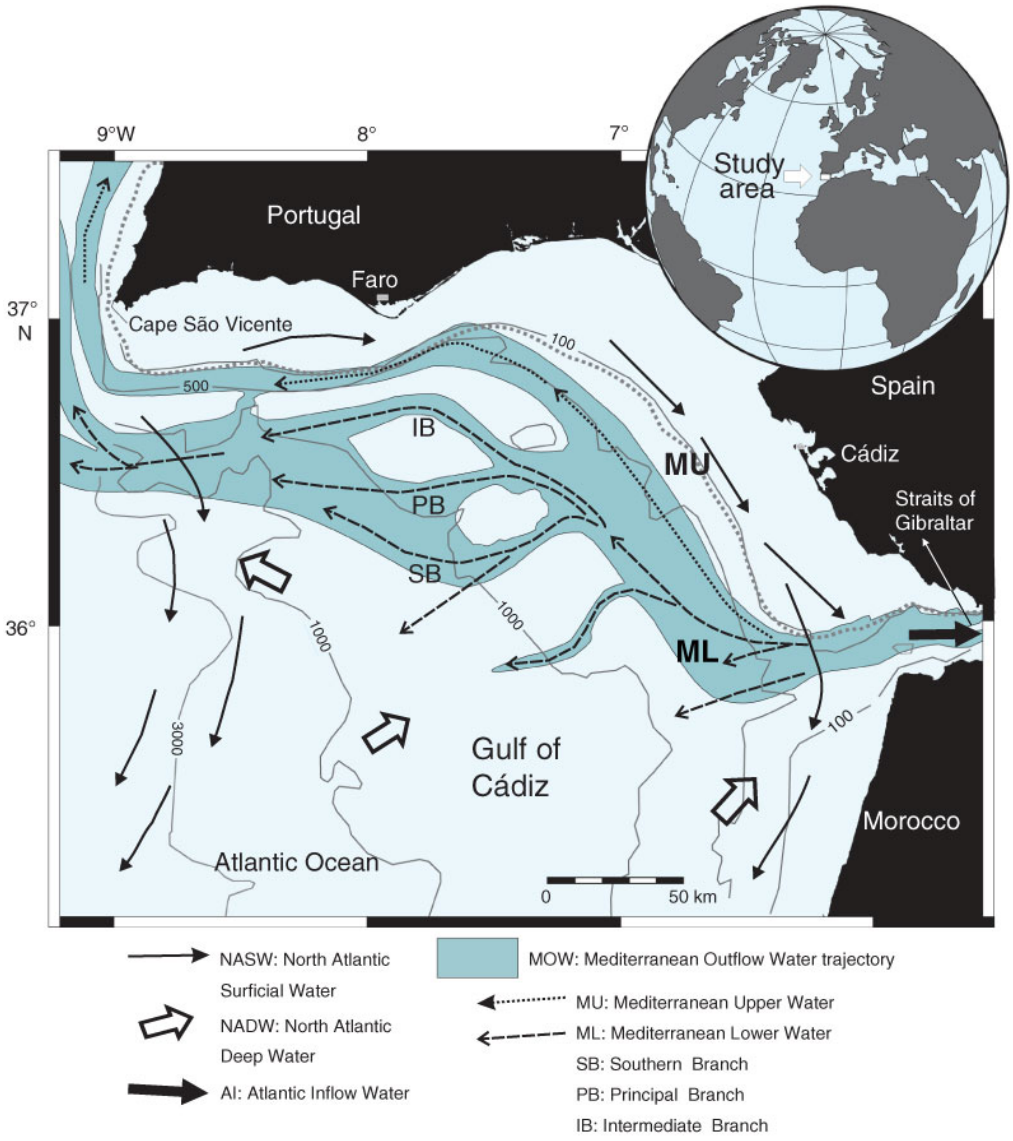

Figure 2 - Path taken by the MOW following exit from the Straits of Gibraltar, from IODP Exp. 339 Proceedings

After exiting at the Straits of Gibraltar, the MOW mixes with the North Atlantic Central Water and reaches a buoyant state around 1100m (Iorga and Lozier, 1999). Flowing into the open Atlantic, this water mass divides into an upper core and a lower core, located at water

depths between 400 and 1400m. The middle continental slope is split into upper and lower terraces, along which the two present-day cores flow (Figure 2). Notably, more mature erosional features and the presence of coarser-grained deposits along the lower terrace suggest stronger currents in the region in the past. Coupled with paleoceanographic data indicating a denser, deeper, and faster MOW in glacial periods, these erosional features are hypothesized to be the result of a period of greater dominance of the MOW's lower core during past glacial stages (Hernandez-Molina et al, 2014).

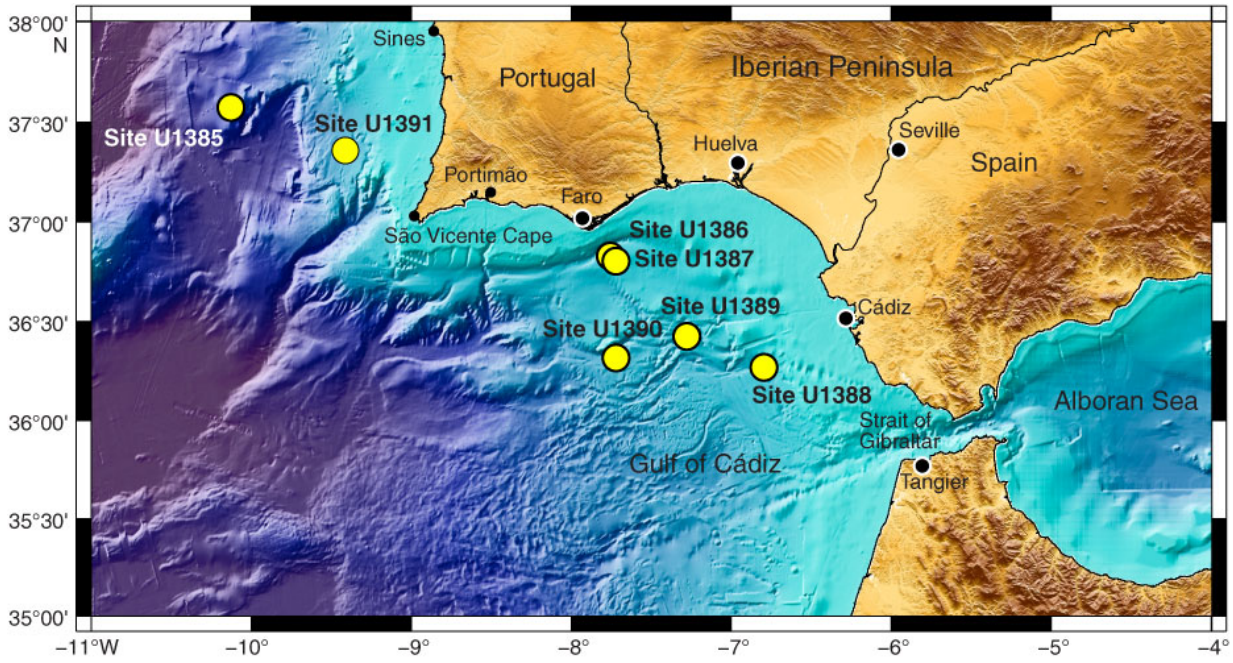

Figure 3 - IODP Expedition 339 Drill Site Locations, from IODP 339 Proceedings

This study examined samples from two sites drilled by IODP Expedition 339: Site U1387 (36°48.321'N; 7°43.1321'W) and Site U1389 (36°25.515′N; 7°16.683′W). Site U1387 is located along the upper terrace, while sediments at Site U1389 record current activity on the lower terrace. The succession examined at both Site U1387 and U1389 is composed of relatively homogenous muddy, silt, and sandy contourites characterized by bigradational grading.

METHODS

Analyses were performed on 40 samples from Site U1389 and 13 samples from Site U1387. Site U1387 samples ranged from a depth of 45.5 to 78.9 meters below sea floor (mbsf) with a sampling interval of ~2.5m while those from Site U1389 ranged from 1.64 to 104.84 mbsf with an interval of ~2.98m. Shipboard data from Exp. 339 defined sedimentation rates using paleomagnetic and biostratigraphic datums. These sedimentation rates were used to construct an age model for sediments based on sampling depth. In the past 300 ky, rates of sedimentation at Site U1387 and Site U1389 remained at a constant 25 cm/ky and 40 cm/ky respectively. The samples from Site U1389 ranged from Recent (3.17) to 226.39 kya, while samples from Site U1389 ranged from 178.76 to 304.57 kya.

Mineralogy of samples was analyzed using powder x-ray diffractometry (XRD). XRD technology uses X-rays that interact with a mineral's crystal structure to define interplanar spacings. These spacings can be used to identify the minerals present in a sample. After being ground using a mortar and pestle, the powdered samples were back-loaded into random mounts, and analyzed using the PANalytical X'Pert Pro XRD in the Subsurface Energy Materials Characterization & Analysis Laboratory (SEMCAL) in the School of Earth Sciences at Ohio State University. Samples were scanned using Ni-filtered CuKα radiation with a step size of 0.020°2θ from 4.0-70.0° at 2s/step. Voltage was set to 45 kV with a current of 20 mA.

PANalytical's HighScore (Plus) and Data Viewer were used to establish the background value on diffraction profiles, as well as to assist with interpreting profiles to identify mineral phases present in samples. Mineral identification was supplemented with peak verification as defined in "Table of Key Lines in X-ray Power Diffraction Patterns of Minerals in Clays and Associated Rocks" (Chen, 1977).

The areas of the 3.04 Å calcite, 7Å chlorite/kaolinite/smectite, 4.26 Å quartz, 4.02 Å plagioclase, and 2.89 Å dolomite peaks were measured using HighScore (Plus). The 10 Å illite peak is expressed as a relatively broad, low-intensity peak in these scans. As a result, this peak area was measured in Data Viewer, which allows a user to select any peak manually to obtain an area measurement. The ratio of a mineral peak area to that of the 4.26 Å quartz peak in the same sample was used to provide a semiquantitative value of mineral abundance. Since this approximation is only relative, abundances cannot be compared between minerals. However, this method does permit discussion of covariations and the relative change of each mineral through time. Replicate analyses were conducted for 4 samples from Site U1389 and the resulting analytical uncertainties are presented in Table 1. No replicates were analyzed for Site U1387, but analytical uncertainties from U1389 are applied to the data from U1387.

Table 1

Analytical uncertainty in intensity ratios - Site U1389

Mineral	Diffraction Peak (Å)	Uncertainty
Calcite	3.04	± 5.93%
Dolomite	2.98	± 6.87%
Illite	10	± 17.89%
Kaolinite/Chlorite/Smectite	7	± 9.82%

Uncertainties are calculated for each mineral as the average of:
[(maximum peak area ratio – mean)/mean peak are ratio] *100
for each 4 pairs of replicate samples.

To examine the variation in mineral abundance over interglacial/glacial timescales, samples were grouped according to benthic $\delta^{18}O$-defined Marine Isotope Stages (MIS) (Lisiecki and Raymo, 2005). These groupings are presented in Appendix A. For the major terrigenous phases, an average mineral/quartz ratio values was calculated for each MIS.

RESULTS

Terrigenous mineral phases present at Site U1387 and Site U1389 include: quartz, calcite, pyrite, dolomite, illite, interstratified clays, and varieties of plagioclase and potassium feldspar. Aragonite was also identified, but may have a biogenic or terrigenous source. Based on initial results, factors such as preferred orientation, mixed-layering, and the absence of analysis following glycolation prohibit distinct identification of the 7Å phyllosilicates (Brindley, 1952). Instead, the 7Å peak is interpreted as a result of the presence of chlorite and/or kaolinite and/or smectite. Changes in the intensity ratios of the major terrigenous mineral phases at Site U1389 through time are presented in Figures 4, 5, 6, and 7. Equivalent data for Site U1387 are presented in Figures 8, 9, 10, and 11. The area under the specific peak for each mineral is presented in Appendix B. Ratios of those peak areas to each sample's 4.26Å quartz peak area are presented in Appendix C. Average intensity ratios, calculated by MIS groupings, are presented in Table 2.

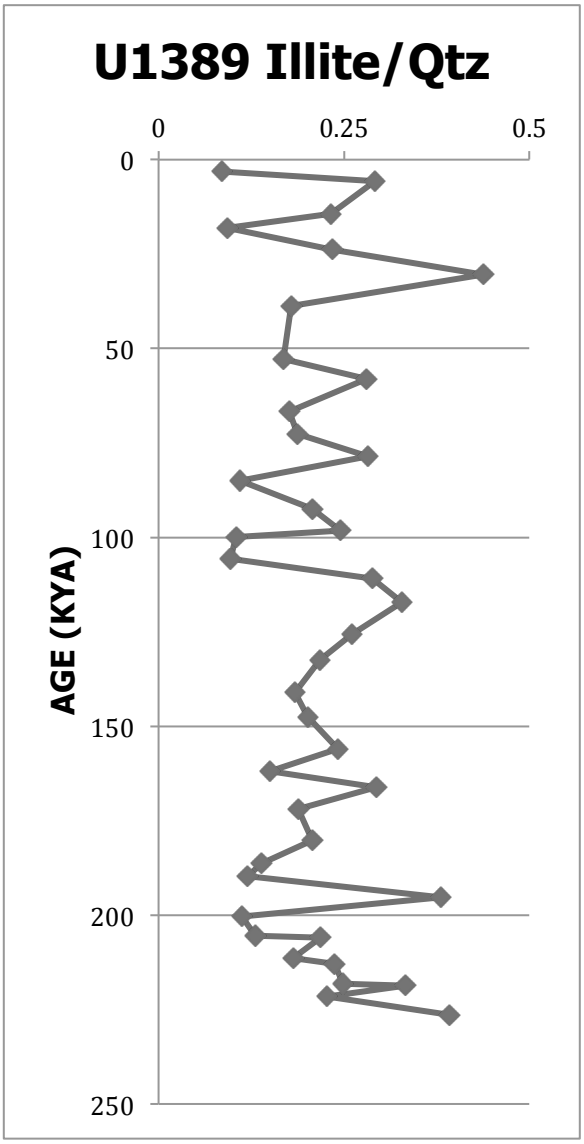

Figure 4 – Illite intensity ratio over the past ~200ky at Site U1389

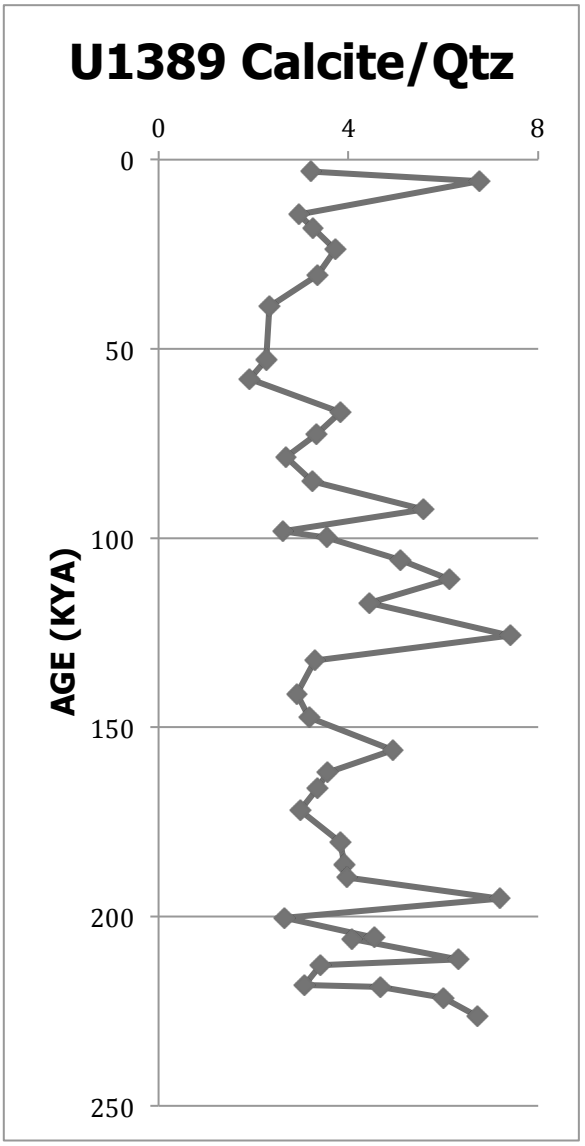

Figure 5 – Calcite intensity ratio over the past ~200ky at Site U1389

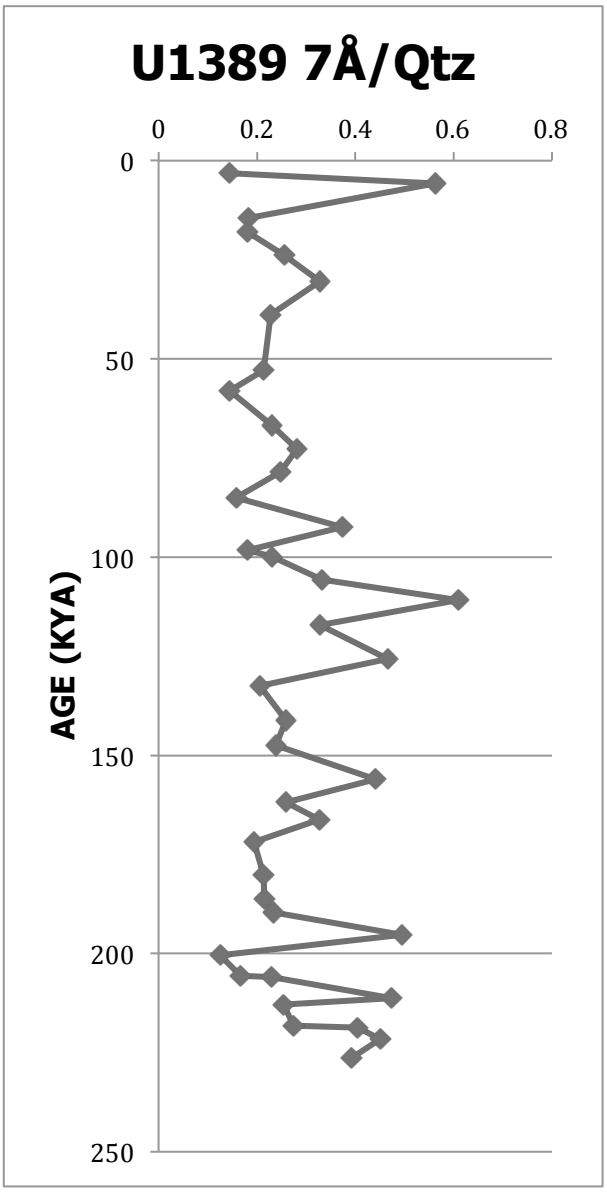

Figure 6 – 7 angstrom peak intensity ratio over the past ~200ky at Site U1389

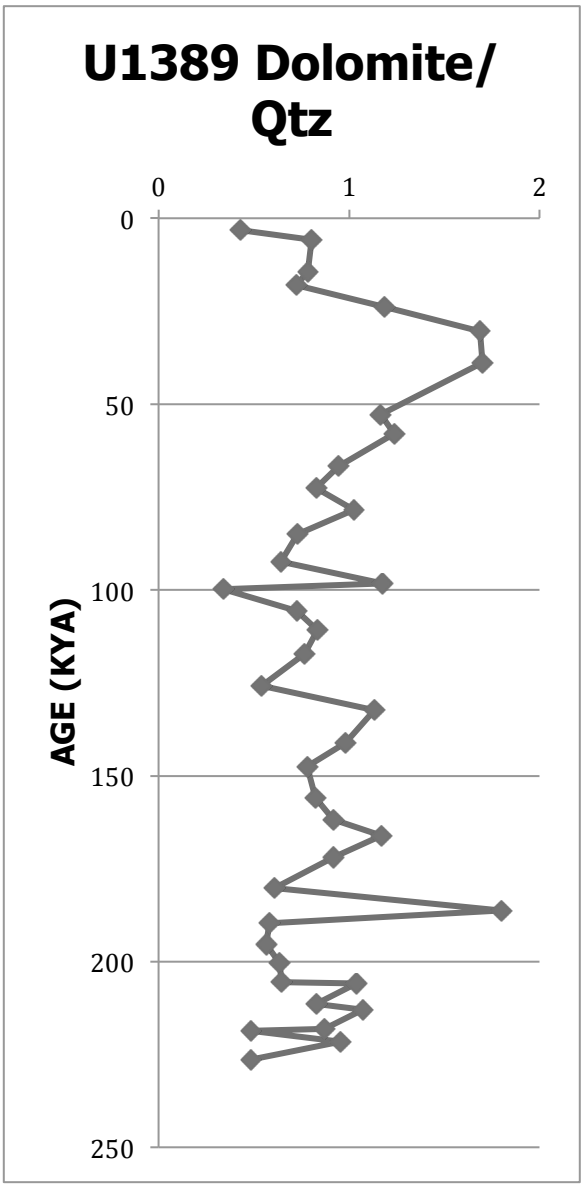

Figure 7 – Dolomite intensity ratio over the past ~200ky at Site U1389

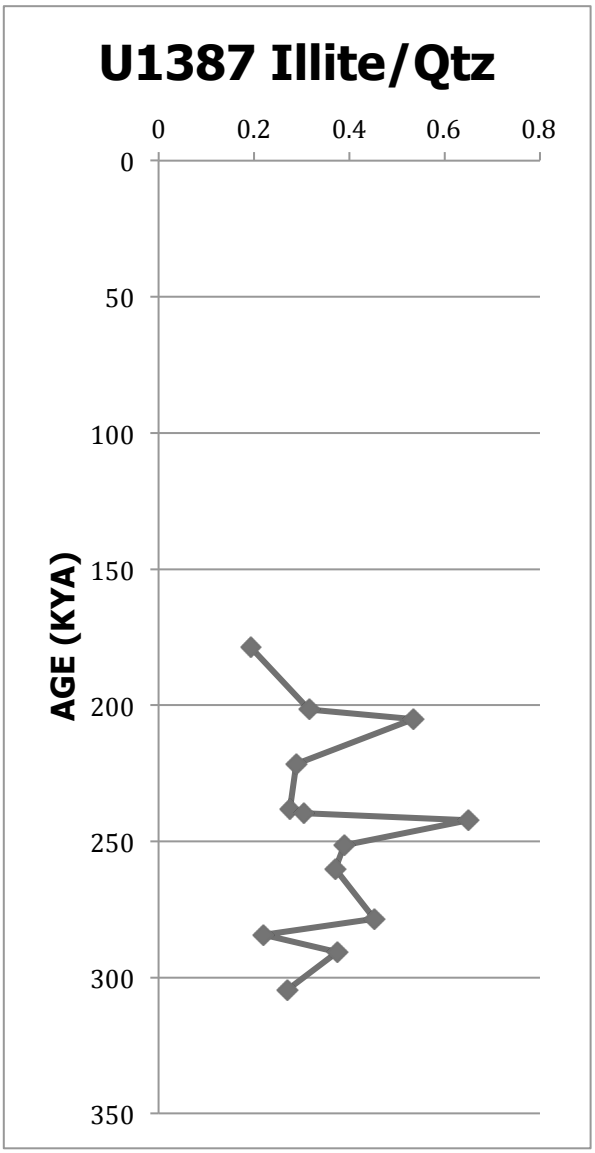

Figure 8 – Illite intensity ratio from ~178 to ~304 kya at Site U1387

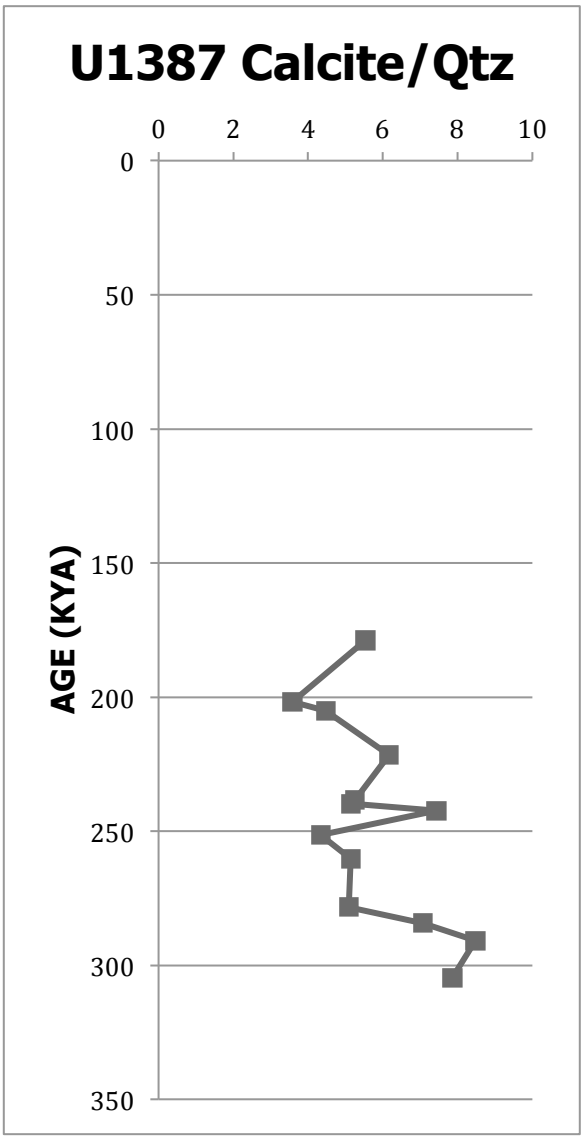

Figure 9 – Calcite intensity ratio from ~178 to ~304 kya at Site U1387

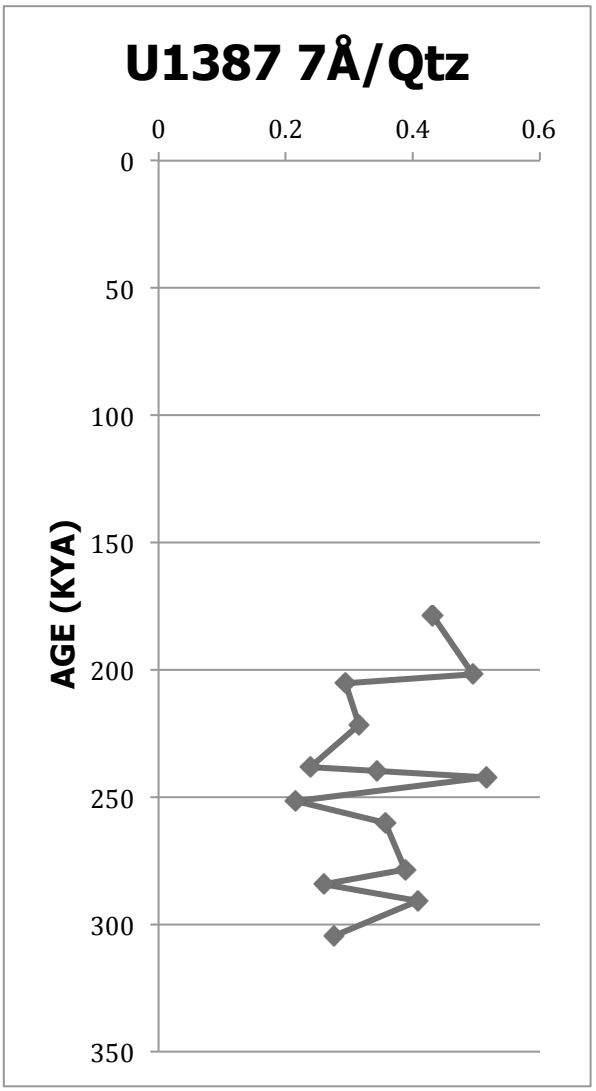

Figure 10 – 7 angstrom peak intensity ratio from ~178 to ~304 kya at Site U1387

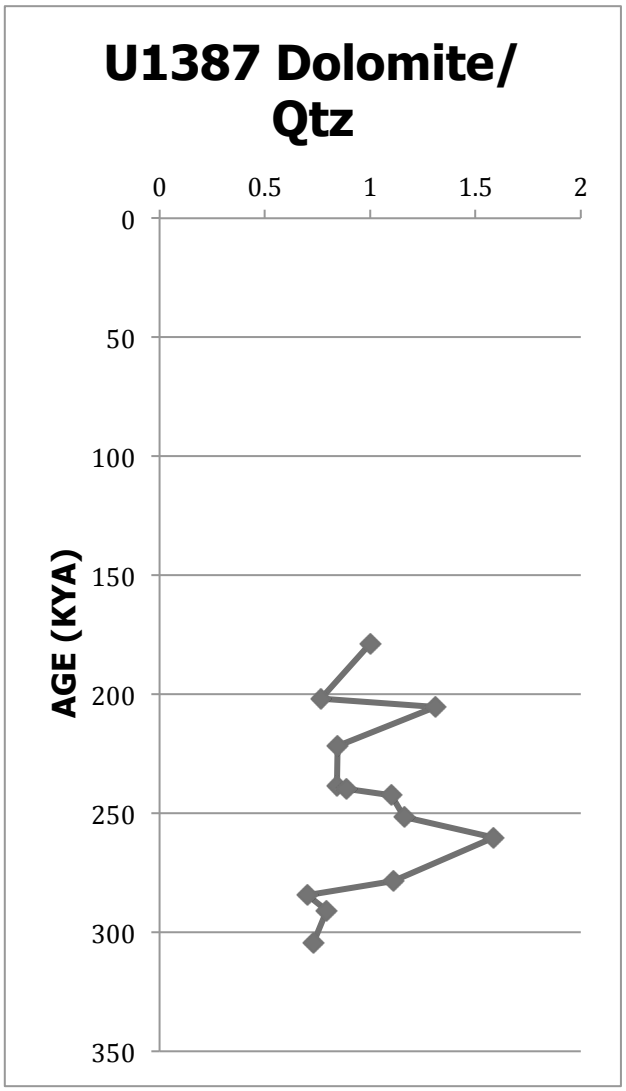

Figure 11 – Dolomite intensity ratio from ~178 to ~304 kya at Site U1387

Table 2

Marine Isotope Stage Averages - Site U1387

MIS	Calcite	Dolomite	Illite	7Å
MIS 6 (n=1)	5.53	1.00	0.19*	0.43
MIS 7	5.34*	0.96	0.39	0.37
MIS 8	6.02*	1.07*	0.36	0.33
MIS 9 (n=1)	7.87	0.73	0.27	0.28

Marine Isotope Stage Averages - Site U1389

MIS	Calcite	Dolomite	Illite	7Å
MIS 1	4.98*	0.62*	0.19	0.35*
MIS 2	3.31*	0.90*	0.19	0.21
MIS 3	2.65	1.52*	0.26	0.26*
MIS 4	2.87*	1.09*	0.23	0.19*
MIS 5	4.41*	0.76*	0.21	0.32*
MIS 6	3.59*	0.97*	0.19	0.26*
MIS 7	4.87	0.76	0.25	0.33

*Change from average value in underlying MIS is outside analytical uncertainty

DISCUSSION

At Site U1389, the calcite/quartz and 7Å/quartz intensity ratios typically exhibit higher values during interglacial stages (odd numbered MIS), although this is not true for calcite/quartz in MIS 4 versus MIS 3. In contrast, dolomite/quartz is generally higher in glacial stages, as are the peak intensities of quartz. The unusually low calcite intensity ratio in MIS 3 may be due to high levels of climate variability during that time, characterized by abrupt warming phases called Dansgaard-Oeschger events (Van Meerbeeck et al., 2009). Furthermore, this also may be due to the combined biogenic and detrital contribution of calcite, compared to the uniquely terrigenous input of the remaining minerals. The Guadalquivir River is interpreted as the primary source of the terrigenous minerals (Verdenius, 1970). The 7Å/quartz intensity ratio changes little from MIS 3 to MIS 2; this signal also may have been affected by the variability in MIS 3. Relative to other MIS pairs (1/2, 4/5), peak area ratios for MIS 3/4 are low and similar to one another. In MIS 3/4, other mineral peak ratios are similar to or greater than their values in 1/2 and 5/6, suggesting that terrigenous input did not decline. With this in mind, it is likely that either biogenic input was lower and less variable, or there was greater dissolution in this time period.

Due to low sample sizes, interpretations are not made for MIS 6 (n=1) and MIS 9 (n=1) at Site U1387. In the only interglacial/glacial pair examined at Site U1387 (MIS 7/8), the calcite/quartz value was higher during the glacial stage. Differences in the remaining intensity ratios were not outside analytical uncertainty for MIS 7 and MIS 8 at this site.

Results from both U1389 and U1387 support a consistent trend in which calcite and the 7Å clays increase when main MOW flow is not present at that site: at U1387 during glacial periods and at U1389 during interglacial periods. In contrast, dolomite and quartz become more abundant during those times of main MOW flow at a site. This relationship suggests preferential

deposition of quartz and dolomite in high velocity settings, with calcite and 7Å clay deposition concentrated in low MOW velocity settings. This control is possibly the result of differences in grain size, in which coarse-grained quartz and dolomite are increasing in abundance due to higher-velocity conditions.

The relationship of higher ratios for some minerals in interglacial stages is not a strong link. The MIS 3/MIS 4 calcite/quartz values and the MIS 2/MIS 3 values for the 7Å/quartz ratio could indicate the absence of a strong linkage between mineral abundance and glacial/interglacial stages, suggesting that mineralogy may not respond significantly on these timescales. This time lag may prevent the use of mineralogy as an effective proxy of bottom-water current core location.

SUGGESTIONS FOR FUTURE WORK

While useful for analyzing trends for individual minerals, semiquantitative abundances are limited because abundances of different minerals cannot be compared. In future studies, sample preparation with an internal standard such as corundum or ZnO would provide mineral abundances in terms of weight percentage and permit a more robust analysis of the variation of minerals through time.

Next, analysis of grain size distributions through time would serve to identify better the controls on preferential deposition of minerals in glacial or interglacial periods.

Finally, recent work (Bahr et al., 2014) has examined the use of XRF scanning data to reconstruct small-scale variability in bottom-water current velocity at Site U1387 in the Gulf of Cadiz for MIS 1–5. Their results have indicated that the Zr/Al ratio can reveal very abrupt shifts in current velocity due to rapid climate change events such as Greenland Stadials and Interstadials. Future work using these IODP cores could benefit from this type of XRF analysis in order to reconstruct high-resolution current velocity beyond MIS 5.

REFERENCES CITED

Bahr, André; Jiménez-Espejo, Francisco J; Kolasinac, Nada; Grunert, Patrick; Hernandéz-Molina, Francisco Javier; Röhl, Ursula; Voelker, Antje HL; Escutia, Carlota; Stow, Dorrik A V; Alvarez Zarikian, Carlos A; Hodell, David A (2014): X-ray fluorescence (XRF) scannings and grain size analysis at sites in the Gulf of Cádiz. PANGAEA, doi:10.1594/PANGAEA.831133, Supplement to: Bahr, André; Jiménez-Espejo, Francisco J; Kolasinac, Nada; Grunert, Patrick; Hernandéz-Molina, Francisco Javier; Röhl, Ursula; Voelker, Antje HL; Escutia, Carlota; Stow, Dorrik A V; Alvarez Zarikian, Carlos A (2014): Deciphering bottom current strength and paleoclimate signals from contourite deposits in the Gulf of Cádiz during the last 140 kyr: an inorganic geochemical approach. Geochemistry, Geophysics, Geosystems, 15(8), 3145-3160, doi:10.1002/2014GC005356.

Brindley, GW. (1952), Identification of Clay Minerals by X-ray Diffraction Analysis, Clays and Clay Minerals, 1, no. 1, pp. 119–129, doi:10.1346/CCMN.1952.0010116.

Bozec, A., M. S. Lozier, E. P. Chassignet, and G. R. Halliwell (2011), On the variability of the Mediterranean Outflow Water in the North Atlantic from 1948 to 2006, J. Geophys. Res., 116, C09033, doi:10.1029/2011JC007191.

Chen, P.Y., 1977, Table of key lines in X-ray powder diffraction patterns of minerals in clays and associated rocks: Geological Survey Occasional Paper 21, Indiana Geological Survey Report 21, 67 pp.

Expedition 339 Scientists (2012), Mediterranean outflow: environmental significance of the Mediterranean Outflow Water and its global implications, IODP Preliminary Report 339, doi:10.2204/iodp.pr.339.2012.

Hernández-Molina, F.J. et al (2014), Onset of Mediterranean outflow into the North Atlantic, Science, 344, p. 1244-1250, doi:10.1126/science.1251306.

Huneke, N.V., D.A.V. Stow (2008), Identification of ancient contourites, problems and palaeoceanographic significance, In: Rebesco, M., A. Camerlenghi (Eds.), Contourites, Developments in Sedimentology, 60, Elsevier, Amsterdam, p. 323–344.

Iorga, M.C. and Lozier, M.S. (1999), Signatures of the Mediterranean outflow from a North Atlantic climatology: 2. Diagnostic velocity fields. Journal of Geophysical Research 104: doi: 10.1029/1999JC900204.

Lee, H., and J. Baraza (1999), Geotechnical characteristics and slope stability in the Gulf of Cadiz, Mar. Geol., 155, p. 173–190.

Lisiecki, L. E., and M. E. Raymo (2005), A Pliocene-Pleistocene stack of 57 globally distributed benthic $\delta^{18}O$ records, Paleoceanography, 20, PA1003, doi:10.1029/2004PA001071.

Penaud, A., Eynaud, F., Turon, J. L., Blamart, D., Rossignol, L., Marret, F., Lopez-Martinez, C., Grimalt, J. O., Malaize, B., and Charlier, K. (2010), Contrasting paleoceanographic conditions off Morocco during Heinrich events (1 and 2) and the Last Glacial Maximum, Quat. Sci. Rev., 29, p. 1923–1939.

Rebesco, M., F. Javier Hernández-Molina, D.V. Rooij, and A. Wåhlin (2014), Contourites and associated sediments controlled by deep-water circulation processes: State-of-the-art and future considerations, Mar. Geol., 352, p.111-154, doi:10.1016/j.margeo.2014.03.011.

Stow, D.A.V, J.C. Faugères (2008), Contourite facies and the facies model, in: M. Rebesco, A. Camerlenghi (Eds.), Contourites, Developments in Sedimentology, 60, Elsevier, Amsterdam, p. 223–256

Van Meerbeeck, C.J., Renssen H., and Roche, D.M. (2009), How did Marine Isotope Stage 3 and Last Glacial Maximum climates differ? Perspectives from equilibrium simulations, Cli. Past, 5, p. 33–51

Verdenius, J.G. (1970), Neogene stratigraphy of the Western Guadalquivir Basin (Southern Spain), Utrecht micropaleontological bulletins, 3, 109 pp.

Viana, A.R.; Rebesco, M. (Ed.) (2007). Economic and palaeoceanographic significance of contourite deposits. Geological Society Special Publication, 276. The Geological Society: London. ISBN 978-1-86239-226-7. 350 pp.

Appendix A

Marine Isotope Stage Sample Groupings - Site U1387

Marine Isotope Stage	Depth (MCD)	Age (kya)
6	49.08	178.76
7	55.37	201.67
	56.34	205.20
	60.84	221.59
	65.41	238.24
	65.79	239.62
	66.54	242.36
8	69.05	251.50
	71.43	260.17
	76.42	278.34
	78.06	284.31
	79.82	290.72
9	83.62	304.57

Marine Isotope Stage Sample Groupings - Site U1389

Marine Isotope Stage	Depth (MCD)	Age (kya)
1	1.64	3.17
	2.96	5.71
2	7.46	14.40
	9.34	18.03
	12.34	23.82
3	15.79	30.48
	20.1	38.80
	27.39	52.88
4	30.04	57.99
	34.57	66.74

Appendix A (continued)

Marine Isotope Stage Sample Groupings - Site U1389

Marine Isotope Stage	Depth (MCD)	Age (kya)
5	37.64	72.66
	40.67	78.51
	44.04	85.02
	47.88	92.43
	50.89	98.24
	51.72	99.85
	54.76	105.71
	57.43	110.87
	60.68	117.14
	65.13	125.73
6	68.59	132.41
	73.12	141.16
	76.37	147.43
	80.79	155.97
	83.84	161.85
	86.07	166.16
	89.04	171.89
	93.39	180.29
	96.48	186.25
	98.23	189.63
7	101.17	195.31
	103.79	200.37
	106.47	205.54
	106.67	205.93
	109.47	211.33
	110.28	212.90
	113	218.15
	113.25	218.63
	114.75	221.53
	117.27	226.39

Appendix B

Mineral Peak Areas - Site U1387

Depth (MCD)	Age (kya)	Quartz	Calcite	Dolomite	Illite	7Å
49.08	178.76	215.82	1192.92	215.95	41.8	93.12
55.37	201.67	265.11	948.72	202.96	83.8	131
56.34	205.20	281.1	1254.69	368.46	150.4	82.7
60.84	221.59	221.35	1365.3	187.11	63.8	69.7
65.41	238.24	253.32	1331.16	213.72	69.7	60.6
65.79	239.62	252.03	1295.67	224.12	76.8	86.6
66.54	242.36	190.12	1412.55	209.16	123.6	98
69.05	251.50	289.05	1253.47	335.47	112.6	62.4
71.43	260.17	286.38	1471.76	454.64	106.2	102.2
76.42	278.34	245.7	1252.12	272.79	111.1	95.2
78.06	284.31	258.94	1829.84	181.89	57.1	67.4
79.82	290.72	210.76	1787.38	167.07	78.9	86
83.62	304.57	217.58	1711.58	158.64	58.9	60

Mineral Peak Areas - Site U1389

Depth (MCD)	Age (kya)	Quartz	Calcite	Dolomite	Illite	7Å
1.64	3.17	409.53	1314.87	176.81	35.1	58.9
2.96	5.71	228.53	1543.19	183.21	66.7	128.5
7.46	14.40	342.48	1014.12	267.75	79.4	62.5
9.34	18.03	331.43	1076.29	239.13	30.6	60.2
12.34	23.82	337.8	1256.13	400.91	79	86.2
15.79	30.48	374.83	1256.16	632.49	164	122.9
20.1	38.80	497.18	1162.46	845.61	88.8	113.2
27.39	52.88	450.45	1018.74	525.24	76	96.1
30.04	57.99	524.77	1004.92	649.02	147.1	75.9
34.57	66.74	317.82	1216.53	300.43	55.9	73.4
37.64	72.66	358.24	1191.29	296.28	67.1	100.6
40.67	78.51	368.56	992.23	377.79	104	91.2
44.04	85.02	344.3	1114.89	250.83	37.9	54.4
47.88	92.43	244.36	1363.38	156.66	50.6	91.4
50.89	98.24	372.55	975.18	438.02	91.2	67.4
51.72	99.85	316.65	1125.89	107.24	33	73.2
54.76	105.71	273.89	1396.53	199.2	26.5	90.9
57.43	110.87	207.62	1271.04	172.74	59.9	126.5
60.68	117.14	327.21	1452.2	251.25	107.2	107.4

Appendix B (continued)

Mineral Peak Areas - Site U1389

Depth (MCD)	Age (kya)	Quartz	Calcite	Dolomite	Illite	7Å
65.13	125.73	191.61	1417.98	103.79	50	89.4
68.59	132.41	389.61	1281.1	440.68	84.7	80.1
73.12	141.16	422.13	1231.85	414.54	77.6	109.6
76.37	147.43	382.35	1214.47	298.46	77	91.2
80.79	155.97	219.32	1082.85	180.33	53.1	96.8
83.84	161.85	286.15	1021.2	262.41	43.1	74
86.07	166.16	363	1212.71	424.8	106.4	118.6
89.04	171.89	350.63	1047.12	322.17	65.9	68.1
93.39	180.29	275.71	1057.32	167.88	57.1	58.9
96.48	186.25	317.65	1241.7	570.65	44.3	68.3
98.23	189.63	338.31	1339.86	197.22	40.6	78.8
101.17	195.31	171.83	1235.82	96.9	65.4	85
103.79	200.37	354.82	944.16	224.97	40	44.3
106.47	205.54	342.43	1555.76	220.66	44.6	57.3
106.67	205.93	341.55	1389.99	354.58	74.6	78.4
109.47	211.33	191.16	1205.58	158.27	34.7	90.5
110.28	212.90	332.82	1134.94	356.45	78.9	84.4
113	218.15	253.8	782.3	220.95	63	69.8
113.25	218.63	243.58	1138.47	117.83	81.2	98.6
114.75	221.53	250.48	1502.84	238.86	56.9	112.9
117.27	226.39	220.77	1484.57	106.88	86.5	86.4

Appendix C

Mineral/Quartz Ratios - Site U1387

Depth (MCD)	Age (kya)	Calcite/Qtz	Dolomite/Qtz	Illite/Qtz	7Å/Qtz
49.08	178.76	5.53	1.00	0.19	0.43
55.37	201.67	3.58	0.77	0.32	0.49
56.34	205.20	4.46	1.31	0.54	0.29
60.84	221.59	6.17	0.85	0.29	0.31
65.41	238.24	5.25	0.84	0.28	0.24
65.79	239.62	5.14	0.89	0.30	0.34
66.54	242.36	7.43	1.10	0.65	0.52
69.05	251.50	4.34	1.16	0.39	0.22
71.43	260.17	5.14	1.59	0.37	0.36
76.42	278.34	5.10	1.11	0.45	0.39
78.06	284.31	7.07	0.70	0.22	0.26
79.82	290.72	8.48	0.79	0.37	0.41
83.62	304.57	7.87	0.73	0.27	0.28

Mineral/Quartz Ratios - Site U1389

Depth (MCD)	Age (kya)	Calcite/Qtz	Dolomite/Qtz	Illite/Qtz	7Å
1.64	3.17	3.21	0.43	0.09	0.14
2.96	5.71	6.75	0.80	0.29	0.56
7.46	14.40	2.96	0.78	0.23	0.18
9.34	18.03	3.25	0.72	0.09	0.18
12.34	23.82	3.72	1.19	0.23	0.26
15.79	30.48	3.35	1.69	0.44	0.33
20.1	38.80	2.34	1.70	0.18	0.23
27.39	52.88	2.26	1.17	0.17	0.21
30.04	57.99	1.91	1.24	0.28	0.14
34.57	66.74	3.83	0.95	0.18	0.23
37.64	72.66	3.33	0.83	0.19	0.28
40.67	78.51	2.69	1.03	0.28	0.25
44.04	85.02	3.24	0.73	0.11	0.16
47.88	92.43	5.58	0.64	0.21	0.37
50.89	98.24	2.62	1.18	0.24	0.18
51.72	99.85	3.56	0.34	0.10	0.23
54.76	105.71	5.10	0.73	0.10	0.33
57.43	110.87	6.12	0.83	0.29	0.61
60.68	117.14	4.44	0.77	0.33	0.33
65.13	125.73	7.40	0.54	0.26	0.47

Appendix C (continued)

Mineral/Quartz Ratios - Site U1389

Depth (MCD)	Age (kya)	Calcite/Qtz	Dolomite/Qtz	Illite/Qtz	7Å
68.59	132.41	3.29	1.13	0.22	0.21
73.12	141.16	2.92	0.98	0.18	0.26
76.37	147.43	3.18	0.78	0.20	0.24
80.79	155.97	4.94	0.82	0.24	0.44
83.84	161.85	3.57	0.92	0.15	0.26
86.07	166.16	3.34	1.17	0.29	0.33
89.04	171.89	2.99	0.92	0.19	0.19
93.39	180.29	3.83	0.61	0.21	0.21
96.48	186.25	3.91	1.80	0.14	0.22
98.23	189.63	3.96	0.58	0.12	0.23
101.17	195.31	7.19	0.56	0.38	0.49
103.79	200.37	2.66	0.63	0.11	0.12
106.47	205.54	4.54	0.64	0.13	0.17
106.67	205.93	4.07	1.04	0.22	0.23
109.47	211.33	6.31	0.83	0.18	0.47
110.28	212.90	3.41	1.07	0.24	0.25
113	218.15	3.08	0.87	0.25	0.28
113.25	218.63	4.67	0.48	0.33	0.40
114.75	221.53	6.00	0.95	0.23	0.45
117.27	226.39	6.72	0.48	0.39	0.39